

LETTER TO THE EDITOR

Caught in the web: galaxy mergers along cosmic filaments

Carolina Dulcien^{1,2,3}, Yara L. Jaffé^{2,3,*}, Jacob P. Crossett², Raúl Baier-Soto^{2,3,4}, Hugo Méndez-Hernández^{5,3}, Christopher P. Haines^{6,3}, Guillermo Cabrera-Vives^{1,3}, Patricio Olivares², P. Vásquez-Bustos⁷, Maria Argudo-Fernández^{7,8}, Javiera Vivanco², Lawrence Bilton^{9,10,11}, Clécio R. Bom¹¹, Giuseppe D’Ago¹², Alexis Finoguenov¹³, Ulrike Kuchner¹⁴, Ciria Lima-Dias⁵, Paola Merluzzi¹³, Antonela Monachesi⁵, Diego Pallero^{2,3}, Nicolas Tejos⁴, Gabriel S. M. Teixeira¹¹, Cristóbal Sifón⁴, Maiara S. Carvalho¹⁶, Ricardo Demarco¹⁷, Eduardo Ibar^{9,3}, Gissel P. Montaguth¹⁶, Franco Piraino-Cerda^{2,3,4}, Umberto Rescigno⁶, Vitor Sampaio^{2,3}, Gustavo B. Oliveira Schwarz¹⁸, Rory Smith^{2,3}, Benedetta Vulcani¹³, and Nicola Malavasi¹⁹

(Affiliations can be found after the references)

Received March XX, 2025; accepted MXXX

ABSTRACT

Context. Galaxy clusters grow through the accretion of galaxies from groups, filaments, and other clusters. During this process, galaxies may undergo pre-processing in lower-density environments, where galaxy–galaxy mergers and other interactions can significantly alter their properties prior to cluster infall.

Aims. We investigate the role of galaxy mergers in the pre-processing of galaxies prior to cluster infall by studying the spatial distribution of galaxy mergers across the cosmic web.

Methods. We use a sample of 43,922 galaxies being targeted by the 4MOST CHANCES survey in and around 33 low-redshift clusters ($z < 0.07$). Using Zoobot, a deep-learning framework trained on Galaxy Zoo data, we identify 698 galaxy mergers. We measure their distances to cosmic web filaments and compare it to those of non-merging galaxies.

Results. We find that galaxy mergers are significantly closer to filaments than the non-merging galaxy population, with this trend being strongest beyond the cluster virial radius. This suggests that filaments provide conditions conducive to mergers, possibly moderating relative velocities and enhancing gas availability.

Conclusions. Our findings support a scenario in which filaments play a key role in transforming (pre-processing) galaxies by promoting mergers before entering the cluster cores where star formation quenches.

Key words. Galaxy mergers – Large scale structures – Galaxy evolution

1. Introduction

Understanding galaxy evolution requires considering both intrinsic properties and the environment in which galaxies reside. In the current cosmological framework—the hierarchical structure formation paradigm—cosmic structures grow via the gravitational merging of smaller units over time. This process builds the large-scale structure (LSS) of the Universe: from galaxies to groups, and ultimately, massive galaxy clusters interconnected by filaments and separated by voids (White & Rees 1978; Press & Schechter 1974). Observations provide compelling evidence for hierarchical growth, where galaxies are accreted along filaments into larger systems (Zwicky 1933; Eke et al. 1996).

A wide array of physical mechanisms influence galaxy properties throughout this hierarchical growth. These include internal processes, such as star formation and AGN feedback, as well as environmental effects like gas stripping via ram-pressure from the intracluster medium, tidal interactions, and galaxy-galaxy mergers (Boselli & Gavazzi 2006; Alonso et al. 2007; Darg et al. 2010; Weigel et al. 2018; Ellison et al. 2019). Each of these can significantly alter a galaxy’s morphology, star formation activity, and gas content, contributing to the broad diversity observed in the galaxy population today. Mergers can alter the kinematics of galaxies (including spin orientation), reshape galactic disks, trigger intense starburst events, and feed central supermas-

sive black holes, potentially igniting AGN activity (Toomre & Toomre 1972; Barnes & Hernquist 1992; Hopkins et al. 2006; Cox et al. 2006; Welker et al. 2014; Barsanti et al. 2025).

These environmental mechanisms are expected to act in different locations of the cosmic web. In dense cluster cores for instance, galaxies experience significant gas removal through ram-pressure stripping (Jaffé et al. 2015; Cortese et al. 2021). However, a substantial fraction of galaxies enter clusters already quenched, suggesting that they undergo “pre-processing” in lower-density environments prior to cluster infall (Fujita 2004; Haines et al. 2015; Lopes et al. 2024).

In intermediate-density environments (such as galaxy groups or the outskirts of clusters), mechanisms such as galaxy-galaxy mergers are expected to be more effective, as the lower relative velocities facilitate gravitational binding (Boselli & Gavazzi 2006). Recent observational results using deep learning classifications (Omori et al. 2023) show that merger incidence increases in lower-density environments on scales of 0.5–0.8 h^{-1} Mpc compared to dense environments. This is supported by simulations, which indicate that galaxy mergers preferentially occur in environments with lower relative velocities, such as intermediate-mass haloes, rather than in massive cluster cores (Jian et al. 2012).

Despite this framework, observational studies of mergers at filament-cluster interfaces remain limited, with the specific role

* e-mail: yara.jaffe@usm.cl

of mergers in the pre-processing of galaxies along filaments unexplored systematically.

In this work, we explore the role of galaxy mergers in the pre-processing of galaxies falling into clusters. As the main channel of galaxy accretion into clusters is through large-scale filaments (Cautun et al. 2014), we focus our analysis on the distribution of galaxy mergers relative to filaments feeding clusters. Specifically, we investigate whether galaxy mergers tend to occur along filamentary structures and how this tendency varies with distance from the cluster centre. Throughout this paper, R_{200} refers to the radius within which the mean density is 200 times the critical density at the cluster's redshift. We adopt a Planck 2020 cosmology with $H_0 = 67.4 \text{ km s}^{-1} \text{ Mpc}^{-1}$ and $\Omega_m = 0.315$.

2. Dataset

2.1. Cluster and Galaxy sample

This paper focuses on galaxies in clusters at $z < 0.07$ from the Low- z sub-survey of the 4MOST CHileAN Cluster galaxy Evolution Survey (CHANCES; Haines et al. 2023; Sifón et al. 2025). This survey is tailored to study galaxy pre-processing and will obtain $\sim 500,000$ spectra of galaxies within and around more than 100 clusters out to $5 \times R_{200}$ at $0 < z < 0.45$ with the 4MOST instrument on the 4-m VISTA telescope (de Jong et al. 2019), down to low stellar masses ($m_r < 20.4 \text{ mag}$).

2.2. Large scale environment of galaxies

To characterize galaxy environment we focus on galaxies out to $5 \times R_{200}$ from the cluster centre, selected using photometric redshifts from the DESI Legacy Surveys Data Release 10 (LS-DR10; Zhou et al. 2021), following the CHANCES target selection strategy, which selects cluster galaxies in redshift slices centered on each cluster redshift (see Méndez-Hernández et al. 2026, for details). For the environmental characterization, we limit the sample to galaxies brighter than $m_r = 18.5 \text{ mag}^1$, where the completeness and purity in the selection of cluster members is high ($\sim 80\%$) thanks to the reduced photometric redshift uncertainty ($\langle \sigma_z \rangle \approx 0.145$ for LS-DR10, and $\langle \sigma_z \rangle \approx 0.044$ for our improved LS-DR10-CBPF estimates; see Méndez-Hernández et al. 2026). Using this magnitude range, Baier-Soto et al. (2025) has shown already that filaments can be adequately identified with photometric members.

Filament identification was performed in 2D using the Discrete Persistence Structures Extractor (DisPerSE²; Sousbie 2011), which is widely used for detecting cosmic web components in observations (Bonjean et al. 2020) and simulations (Galárraga-Espinosa et al. 2020; Kuchner et al. 2020; Kraljic et al. 2020; Malavasi et al. 2022). We applied boundary conditions for smooth Delaunay tessellation, with persistence threshold at 3σ and smoothness level of 20 following Baier-Soto et al. (2025). Galaxy-filament distances (D_{fil}) were computed via the point-line method (See Appendix A) along with the projected distance to the cluster centre (r_{cl}).

2.3. Galaxy morphology

To obtain morphological information for the photometric members, we cross-matched the CHANCES catalogue of target galaxies with catalogues containing data from Galaxy Zoo DESI (GZDESI; Walmsley et al. 2023b), which provides automated

morphology measurements based on deep images from the DESI Legacy Imaging Surveys DR8 (DESI-LS-DR8; Dey et al. 2019). The GZDESI morphologies are derived using Zoobot (Walmsley et al. 2023a), a deep learning model trained to replicate the consensus of the Galaxy Zoo volunteer classifications. For each galaxy, Zoobot predicts vote fractions: the expected proportion of human classifiers who would select a given morphological label (e.g., "smooth" or "featured").

While not all galaxies in the CHANCES Low- z survey had a match in the morphological catalogues of GZDESI (since CHANCES is based on DESI LS-DR10 rather than DR8 used for GZDESI), 43,922 galaxy matches were found spread across 33 different clusters (note that 8 clusters are not fully covered by GZDESI, see blue points in Fig. D.1).

This sample of galaxies represents the general galaxy population (which includes both merging and non-merging galaxies).

To identify galaxies undergoing mergers using the GZDESI classifications we consider the vote fractions predicted by Zoobot in the following categories: merger (M-M), major disturbance (M-D), minor disturbance, and none. We visually inspected galaxies with different vote fractions for a random subsample of 2,000 galaxies to define a threshold that allowed us to build a reliable galaxy-galaxy merger sample. We adopted the following thresholds:

$$F_{MM} \geq 0.5 \text{ or } F_{MD} \geq 0.5,$$

where F_{MM} and F_{MD} correspond to the predicted vote fractions for the M-M and M-D cases respectively³. These thresholds yield a high purity (78%) at the expense of completeness (45%), which translates into a selection of clear cases of major mergers or disturbances. To ensure this level of purity, we excluded galaxies with minor disturbances or no signs of interaction, which would dilute the sample.

A total of 698 galaxy mergers were identified, corresponding to $\sim 2\%$ of the sample, implying that the remaining 43,224 galaxies are classified as non-mergers. This merger fraction is low, but expected in cluster environments (see e.g. Kim et al. 2024), and even more so given our conservative criteria for selecting mergers. Figure B.1 shows a few randomly selected example galaxies classified as mergers.

3. Results: Distribution of Mergers across the cosmic web

To determine whether galaxy mergers contribute to the pre-processing of galaxies in filaments before they enter clusters, we compare their spatial distribution in the cosmic web to that of the general galaxy population (43,922 galaxies). This reference sample includes mergers, allowing us to test whether they exhibit distinct environmental preferences using the Anderson-Darling k-sample (AD) test.

Figure 1 shows the distribution of D_{fil} for all merging galaxies compared to the general galaxy population, across different regions: the entire region analyzed ($r < 5 \times R_{200}$), in the cluster region ($r < R_{200}$), and in the cluster outskirts ($R_{200} < r < 5 \times R_{200}$). In two cases, galaxy mergers are preferentially located closer to the filaments than the general galaxy population, with the difference being more pronounced outside the virialized region of the cluster, where merging galaxies have a median filament distance of $0.406^{+0.029}_{-0.024} \text{ Mpc}$, compared to $0.459^{+0.005}_{-0.004} \text{ Mpc}$ for the non-merging galaxies, as shown in the right panel of

³ Note that our conclusions are insensitive to the exact merger probability threshold, remaining stable for values between $F = 0.3-0.6$. Higher thresholds are primarily limited by small-number statistics.

¹ This limit corresponds to $\log_{10}(M_*/M_\odot) \sim 9$

² <https://www2.iap.fr/users/sousbie/disperse.html>

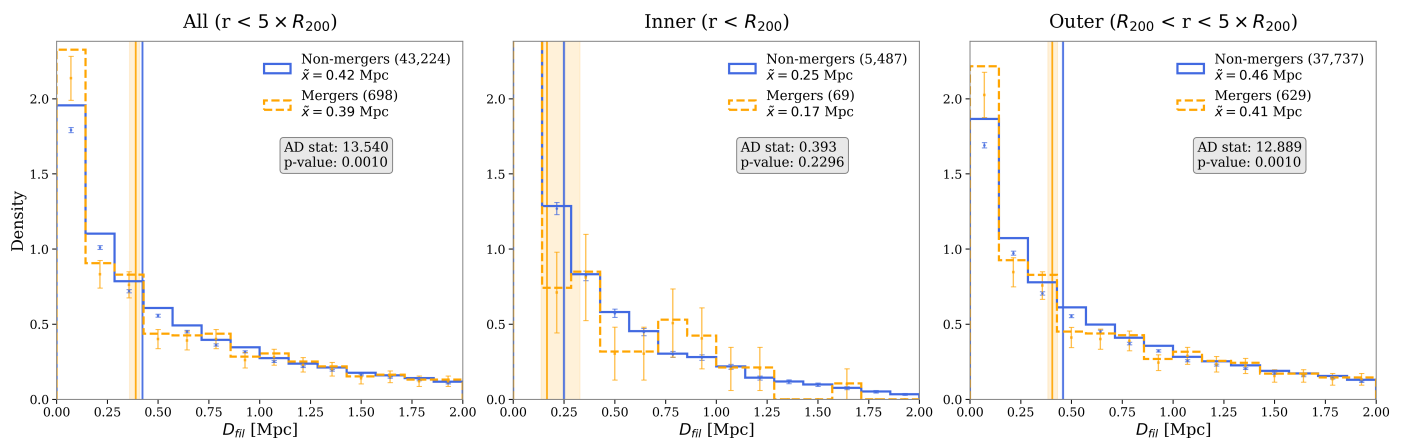


Fig. 1. Normalized distribution of D_{fil} for all merging galaxies (orange dashed line), compared to the non-merging galaxy population (blue dotted line). Left: Distribution for galaxies across the entire cluster region ($r < 5 \times R_{200}$); Middle: galaxies in the inner cluster region ($r < R_{200}$). Right: galaxies in the cluster outskirts ($R_{200} < r < 5 \times R_{200}$). For visualization, distances to filaments are truncated at 2 Mpc, beyond which the galaxy density drops consistently below ~ 0.2 . Error bars correspond to Poisson uncertainties in each bin, while vertical lines mark the median of each distribution. Shaded regions indicate the 68% bootstrap confidence intervals (percentiles 16–84) around the median. The AD statistics and p-values comparing both distributions are shown in the legend. The AD statistics show that galaxy mergers are preferentially located closer to filaments than non-merging galaxies, both at all radii and specifically outside the virial region. Distances to filaments are truncated at 2 Mpc in the plots for visibility, although the full distributions extend up to ~ 4 Mpc.

Figure 1. The quoted uncertainties correspond to the 16th–84th percentiles derived from 1000 bootstrap resamplings (1σ confidence intervals).

While the difference in the medians is small, the difference in the shape of the distributions has statistical significance according to the AD test which yields p-values well below 0.07⁴ outside the virial region. Considering that the typical filament thickness is $\sim 0.7 - 1$ Mpc (e.g., Tempel et al. 2014; Kuchner et al. 2020) this result suggests that mergers are more likely to occur within the filamentary structures themselves. The fact that the trend is more pronounced in the cluster outskirts is not surprising, as the relative velocities between galaxies there are low enough to allow mergers. Hence in the rest of the analysis, we consider only the outer regions of clusters. However, we assessed possible edge effects on the filament detections by redoing the analysis considering an area limited to $r < 4.8 \times R_{200}$, and we obtained the same results and significance.

We also note that the mass distributions of the merger and non-merger samples are very similar but not statistically identical. Nonetheless, we have checked that our results do not change when matching the stellar mass distributions (see Appendix C).

When examining the distribution of mergers cluster-by-cluster (shown in Figure D.2), we found statistically suggestive evidence ($p < 0.07$) that mergers preferentially occur near filaments in $\sim 39\%$ of our sample in the outer regions. For the remaining clusters, although visual inspection suggests similar distribution patterns to those with statistically significant results, the limited number of identified mergers prevents these trends from reaching statistical significance.

Abell 85, a massive relaxed cluster in our sample, provides the strongest example of merger-filament connection, as shown in Figure 2. In this cluster, mergers clearly trace the filamentary structure, supported by statistical indicators including a p-value

⁴ We employ a significance threshold of $\alpha = 0.07$ for our AD tests to account for the inherent observational bias toward filamentary environments present in both samples. This threshold enhances our sensitivity to detect merger-specific spatial deviations while maintaining statistical rigor (false-positive rate of 7%).

of 0.001 and a median distance difference of 0.29 Mpc between merging galaxies and the general population.

Our results suggest that filamentary structures play an important role in galaxy evolution by facilitating merger events that may contribute to the pre-processing of galaxies before they fully enter the cluster environment.

4. Discussion

We find a clear spatial association between galaxy mergers and the filamentary structure of the cosmic web—the first direct observational evidence of enhanced merger activity along cluster-feeding filaments. This connection is strongest beyond the virial radius, where lower relative velocities and the filamentary geometry likely promote gravitational interactions. Thus, filaments not only channel galaxies into clusters but also serve as active sites of pre-processing through mergers.

Our findings agree with simulations predicting enhanced merger activity, morphological transformation, and spin reorientation within filaments (Welker et al. 2014; Dubois et al. 2014; Kuutma et al. 2017; Singh et al. 2020), and they confirm previous indirect observational hints (Malavasi et al. 2016; Mesa et al. 2018; Omori et al. 2023; Rong et al. 2024).

Our analysis is nevertheless subject to several limitations. Filament reconstruction relies on projected galaxy distributions and photometric redshifts, so line-of-sight uncertainties and shot noise may blur filament positions and dilute the signal. Moreover, our conservative merger selection prioritizes purity over completeness, likely underestimating the true merger incidence. Future studies using spectroscopy and more detailed merger identification will help confirm our results.

5. Conclusions

We have investigated the role of cosmic filaments in promoting galaxy mergers as part of the pre-processing of galaxies prior to their infall into clusters. Using a sample of $\sim 40,000$ galaxies in and around 33 low-redshift ($z < 0.07$) clusters from the CHANCES survey, we study the spatial distribution of mergers

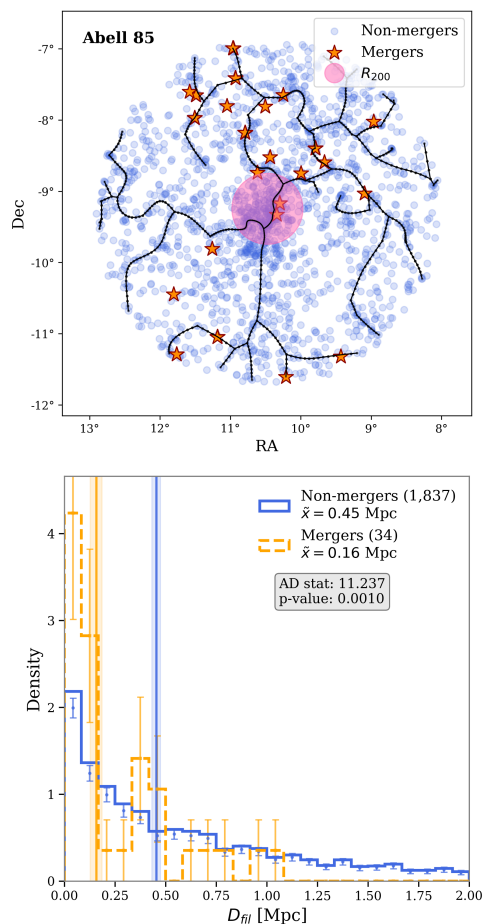


Fig. 2. Distribution of galaxy mergers in the example cluster Abell 85. Top: Spatial distribution of galaxies in the cluster out to $5R_{200}$ showing merging galaxies (orange stars) and non-merging galaxies (blue dots) relative to intracluster filaments (black lines). The pink circle denotes the R_{200} radius for reference. Bottom: Normalized distribution of D_{fil} , comparing merging galaxies (orange) with the non-merging galaxy population (blue) at $r < 5 \times R_{200}$. Symbols are as in Figure 1. In this cluster mergers are significantly closer to filaments by a factor of 2.6 compared with non-merging galaxies.

across the cosmic web. Our main finding is that galaxy mergers are preferentially located near filaments outside the virial region of clusters.

These results provide evidence that cosmic filaments are not merely passive conduits of galaxy infall but active sites of transformation, where mergers contribute to the pre-processing of galaxies prior to cluster infall.

In future work, we aim to expand this analysis using the full CHANCES sample through a dedicated citizen science project that incorporates additional physical mechanisms at play. We will also enrich the analysis with 4MOST spectroscopy, more complex local and global environmental metrics, and comparisons with cosmological hydrodynamical simulations, which can help constrain the underlying physical drivers of filament-driven evolution. Moreover, we will explore whether mergers preferentially occur within galaxy groups/substructures embedded in filaments, comparing the impact of local and LSS-environment, once CHANCES provides robust group/substructures catalogues and central/satellite classifications.

Acknowledgements. YLJ and RS acknowledge support from Agencia Nacional de Investigación y Desarrollo (ANID) through FONDECYT Reg-

ular projects 1241426 and 1230441. YLJ, CD, HMH, CPH, RBS, FPC, EI, VMS, RS and DP gratefully acknowledge financial support from the Millennium Science Initiative Program NCN2024_112. YLJ, RBS, HMH, AM, RD gratefully acknowledge support from the ANID BASAL project FB210003. RBS acknowledges support from ANID/Subdirección de Capital Humano/Doctorado Nacional/2023-21231017. PVB and MAF acknowledge support from the research project PID2023-150178NB-I00 and PID2023-149578NB-I00, financed by MCIN/AEI/10.13039/501100011033, the project A-FQM-510-UGR20 financed from FEDER/Junta de Andalucía-Consejería de Transformación Económica, Industria, Conocimiento y Universidades/Proyecto, by the grants P20_00334 and FQM108, financed by the Junta de Andalucía (Spain), the Emergia program (EMERGIA20_38888) from Junta de Andalucía, and the Grant AST22-4.4, funded by Consejería de Universidad, Investigación e Innovación and Gobierno de España and Unión Europea - NextGenerationEU. CPH acknowledges support from ANID through Fondecyt Regular project number 1252233. HMH acknowledges support from ANID through Fondecyt project 3230176. AM acknowledges support from the ANID FONDECYT Regular grant 1251882, and funding from the HORIZON-MSCA-2021-SE-01 Research and Innovation Programme under the Marie Skłodowska-Curie grant agreement number 101086388. MSC acknowledges support from São Paulo Research Foundation (FAPESP) grant 2023/10774-5 and funding to the S-PLUS project through the process 2019/26492-3. EI gratefully acknowledges financial support from ANID FONDECYT Regular 1221846. CLD acknowledges support from the ANID through Fondecyt project 3250511. GD acknowledges support from UKRI-STFC grants: ST/T003081/1 and ST/X001857/1. We thank A. J. Koch-Hansen, S. Barsanti and A. Fritz for useful comments.

References

- Alonso, M. S., Lambas, D. G., Tissera, P., & Coldwell, G. 2007, *MNRAS*, 375, 1017
- Baier-Soto, R., Jaffé, Y., Finoguenov, A., et al. 2025, *A&A*, 704, A228
- Barnes, J. E. & Hernquist, L. 1992, *ARA&A*, 30, 705
- Barsanti, S., Croom, S. M., Colless, M., et al. 2025, *MNRAS*, 538, 2660
- Bonjean, V., Aghanim, N., Douspis, M., Malavasi, N., & Tanimura, H. 2020, *A&A*, 638, A75
- Boselli, A. & Gavazzi, G. 2006, *PASP*, 118, 517
- Cautun, M., van de Weygaert, R., Jones, B. J. T., & Frenk, C. S. 2014, *MNRAS*, 441, 2923–2973
- Cortese, L., Catinella, B., & Smith, R. 2021, *PASA*, 38, e035
- Cox, T. J., Dutta, S. N., Di Matteo, T., et al. 2006, *ApJ*, 650, 791–811
- Darg, D. W., Kaviraj, S., Lintott, C. J., et al. 2010, *MNRAS*, 401, 1552
- de Jong, R. S., Agertz, O., Berbel, A. A., et al. 2019, *Msngr*, 175, 3
- Dey, A., Schlegel, D. J., Lang, D., et al. 2019, *AJ*, 157, 168
- Dubois, Y., Pichon, C., Welker, C., et al. 2014, *MNRAS*, 444, 1453
- Eke, V. R., Cole, S., & Frenk, C. S. 1996, *MNRAS*, 282, 263
- Ellison, S. L., Viswanathan, A., Patton, D. R., et al. 2019, *MNRAS*, 487, 2491
- Fujita, Y. 2004, *PASJ*, 56, 29
- Galárraga-Espinosa, D., Aghanim, N., Langer, M., Gouin, C., & Malavasi, N. 2020, *A&A*, 641, A173
- Haines, C., Jaffé, Y., Tejos, N., et al. 2023, *Msngr*, 190, 31
- Haines, C. P., Pereira, M. J., Smith, G. P., et al. 2015, *ApJ*, 806, 101
- Hopkins, P. F., Hernquist, L., Cox, T. J., et al. 2006, *ApJS*, 163, 1
- Jaffé, Y. L., Smith, R., Candlish, G. N., et al. 2015, *MNRAS*, 448, 1715
- Jian, H.-Y., Lin, L., & Chiueh, T. 2012, *ApJ*, 754, 26
- Kim, D., Sheen, Y.-K., Jaffé, Y. L., et al. 2024, *ApJ*, 966, 124
- Kraljic, K., Pichon, C., Codis, S., et al. 2020, *MNRAS*, 491, 4294
- Kuchner, U., Aragón-Salamanca, A., Pearce, F. R., et al. 2020, *MNRAS*, 494, 5473
- Kuutma, T., Tamm, A., & Tempel, E. 2017, *A&A*, 600, L6
- Lopes, P. A. A., Ribeiro, A. L. B., & Brambila, D. 2024, *MNRAS*, 527, L19
- Malavasi, N., Arnouts, S., Vibert, D., et al. 2016, *MNRAS*, 465, 3817
- Malavasi, N., Langer, M., Aghanim, N., Galárraga-Espinosa, D., & Gouin, C. 2022, *A&A*, 658, A113
- Méndez-Hernández, H., Lima-Dias, C., Monachesi, A., et al. 2026, *A&A*, 706, A34
- Mesa, V., Duplancic, F., Alonso, S., et al. 2018, *A&A*, 619, A24
- Omori, K. C., Bottrell, C., Walmsley, M., et al. 2023, *A&A*, 679, A142
- Press, W. H. & Schechter, P. 1974, *ApJ*, 187, 425
- Rong, Y., Shen, J., & Hua, Z. 2024, *MNRAS*, 531, L9
- Sifón, C., Finoguenov, A., Haines, C. P., et al. 2025, *A&A*, 697, A92
- Singh, A., Mahajan, S., & Bagla, J. 2020, *MNRAS*, 497, 2265
- Sousbie, T. 2011, *MNRAS*, 414, 350
- Taylor, E. N., Hopkins, A. M., Baldry, I. K., et al. 2011, *MNRAS*, 418, 1587
- Tempel, E., Stoica, R., Martinez, V. J., et al. 2014, *MNRAS*, 438, 3465
- Toomre, A. & Toomre, J. 1972, *ApJ*, 178, 623
- Walmsley, M., Allen, C., Aussel, B., et al. 2023a, *The Journal of Open Source Software*, 8, 5312

- Walmsley, M., Géron, T., Kruk, S., et al. 2023b, MNRAS, 526, 4768
Weigel, A. K., Schawinski, K., Treister, E., Trakhtenbrot, B., & Sanders, D. B. 2018, MNRAS, 476, 2308
Welker, C., Devriendt, J., Dubois, Y., Pichon, C., & Peirani, S. 2014, MNRAS, 445, L46
White, S. D. M. & Rees, M. J. 1978, MNRAS, 183, 341
Zhou, R., Newman, J. A., Mao, Y.-Y., et al. 2021, MNRAS, 501, 3309
Zwicky, F. 1933, Helvetica Physica Acta, 6, 110

-
- ¹ Universidad de Concepción, Víctor Lamas 1290, Barrio Universitario, Concepción, Chile
² Departamento de Física, Universidad Técnica Federico Santa María, Avenida España 1680, Valparaíso, Chile
³ Millennium Nucleus for Galaxies (MINGAL)
⁴ Instituto de Física, Pontificia Universidad Católica de Valparaíso, Casilla 4059, Valparaíso, Chile
⁵ Departamento de Astronomía, Universidad de La Serena, Avda. Raúl Bitrán 1305, La Serena, Chile
⁶ Instituto de Astronomía y Ciencias Planetarias (INCT), Universidad de Atacama, Copayapu 485, Copiapó, Chile
⁷ Departamento de Física Teórica y del Cosmos, Edificio Mecenas, Campus Fuentenueva, Universidad de Granada, E-18071 Granada, Spain
⁸ Instituto Universitario Carlos I de Física Teórica y Computacional, Universidad de Granada, 18071 Granada, Spain
⁹ Instituto de Física y Astronomía, Universidad de Valparaíso, Avda. Gran Bretaña 1111, Valparaíso, Chile
¹⁰ Centre of Excellence for Data Science, Artificial Intelligence & Modelling, The University of Hull, Cottingham Road, Kingston-Upon-Hull, HU6 7RX, UK
¹¹ Centro Brasileiro de Pesquisas Físicas, Rua Dr. Xavier Sigaud 150, Rio de Janeiro, RJ, Brazil
¹² Institute of Astronomy, University of Cambridge, Madingley Road, Cambridge CB3 0HA, United Kingdom
¹³ INAF-Osservatorio Astronomico di Capodimonte, Salita Moiariello 16, I-80134 Napoli, Italy
¹⁴ Department of Physics, University of Helsinki, Gustaf Hällströmin katu 2, 00560 Helsinki, Finland
¹⁵ School of Physics & Astronomy, University of Nottingham, Nottingham NG7 2RD, UK
¹⁶ Departamento de Astronomia, Instituto de Astronomia, Geofísica e Ciências Atmosféricas, Universidade de São Paulo, São Paulo, Brazil
¹⁷ Institute of Astrophysics, Facultad de Ciencias Exactas, Universidad Andrés Bello, Sede Concepción, Talcahuano, Chile
¹⁸ Escola Politécnica, Universidade de São Paulo, Av. Prof. Luciano Gualberto, Travessa do Politécnico 380, São Paulo, Brazil
¹⁹ Max-Planck-Institut für extraterrestrische Physik (MPE), Gießenbachstraße 1, D-85748 Garching bei München, Germany

Appendix A: Schematic view of D_{fil}

We quantified galaxy proximity to large-scale structure using the projected distance to the cluster centre (r_{cl}) and the shortest perpendicular distance to the nearest filament (D_{fil}), calculated via the point-line method where filament segments connect adjacent nodes (See Figure A.1).

In Figure A.1, we illustrate the geometric procedure used to compute the distance D_{fil} between each galaxy and its nearest filament. The filaments are represented as linear segments connecting adjacent nodes, and the minimum galaxy–filament separation is derived using the point–line method described in Section 2.

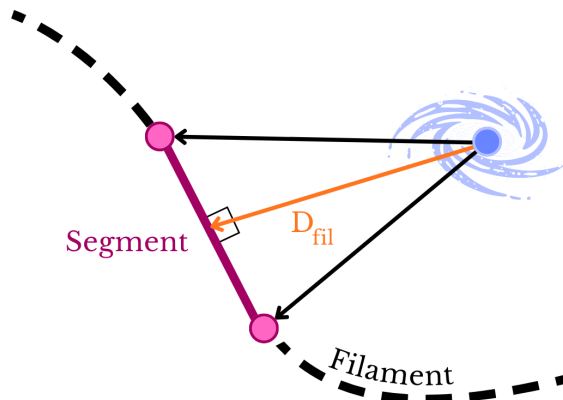


Fig. A.1. Schematic representation of the calculation of the minimum distance (D_{fil}) between a galaxy (blue) and a filament (black dashed curve). The filament is modelled as a set of linear segments (pink line between pink points). The shortest perpendicular distance is computed using the point line method, and is taken as the galaxy–filament distance.

Appendix B: Examples of merger galaxies

In Figure B.1, we show examples of merging galaxies identified with Zoobor (Walmsley et al. 2023a). The top panel displays galaxies selected according to the merger fraction (F_{MM}), while the bottom panel shows those selected based on the major disturbed fraction (F_{MD}), according to the criterion described in Section 3.

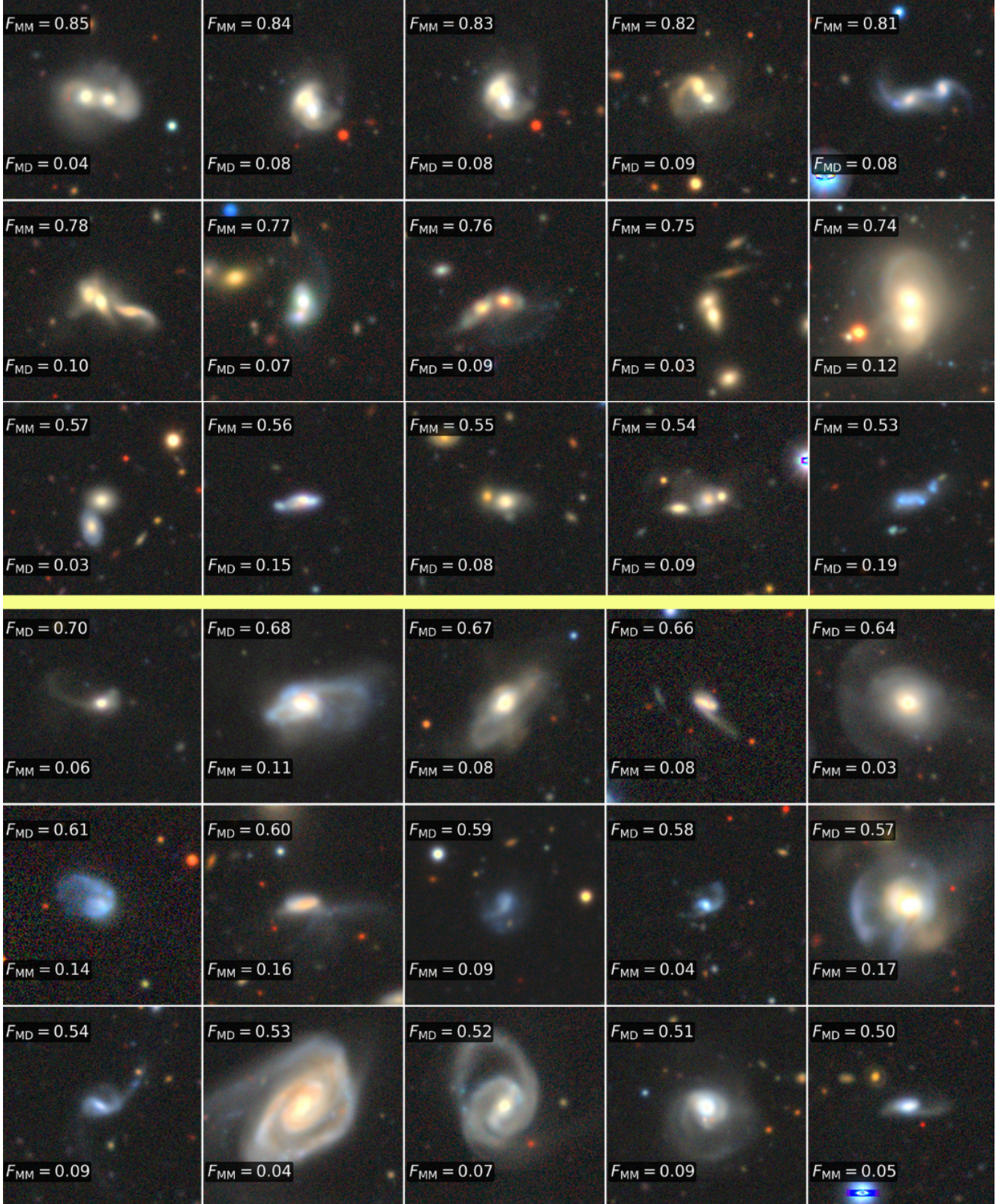


Fig. B.1. Examples of randomly selected merging galaxies. The upper panel shows galaxies selected by F_{MM} , and the bottom panel shows galaxies selected by F_{MD} . In both panels, galaxies are arranged from left to right in decreasing order of the corresponding score.

Appendix C: Controlling for stellar mass

To check that our results are not driven by stellar mass, we have compared the stellar mass distribution of the merger and non-merger galaxy samples. Stellar masses (M_*) were computed following the empirical relation between rest-frame ($g - i$) colour and M_*/L_i in Taylor et al. (2011) for galaxies with reliable photometric measurements (76% of the sample). The remaining objects lack complete photometric coverage in the required filters and therefore lack a stellar-mass estimate. The top panel of Figure C.1 shows that, while the 2 distributions look similar, statistically they are likely to be drawn from the same parent distribution. We checked how these differences could affect our results by repeating the analysis using mass-matched samples. To control for stellar mass without significantly reducing the non-merger sample size, we construct a ratio-matched control sample. Specifically, we bin both populations in stellar mass and randomly down-sample the non-merging galaxies within each mass bin according to the relative merger-to-non-merger ratio, so as to reproduce the shape of the merger mass distribution without enforcing equal sample sizes or up-sampling (see bottom panel of Figure C.1). This procedure is repeated 1000 times using Monte Carlo. Using this mass-controlled sample, we find that the statistical difference in filament distances between mergers and non-mergers remains unchanged.

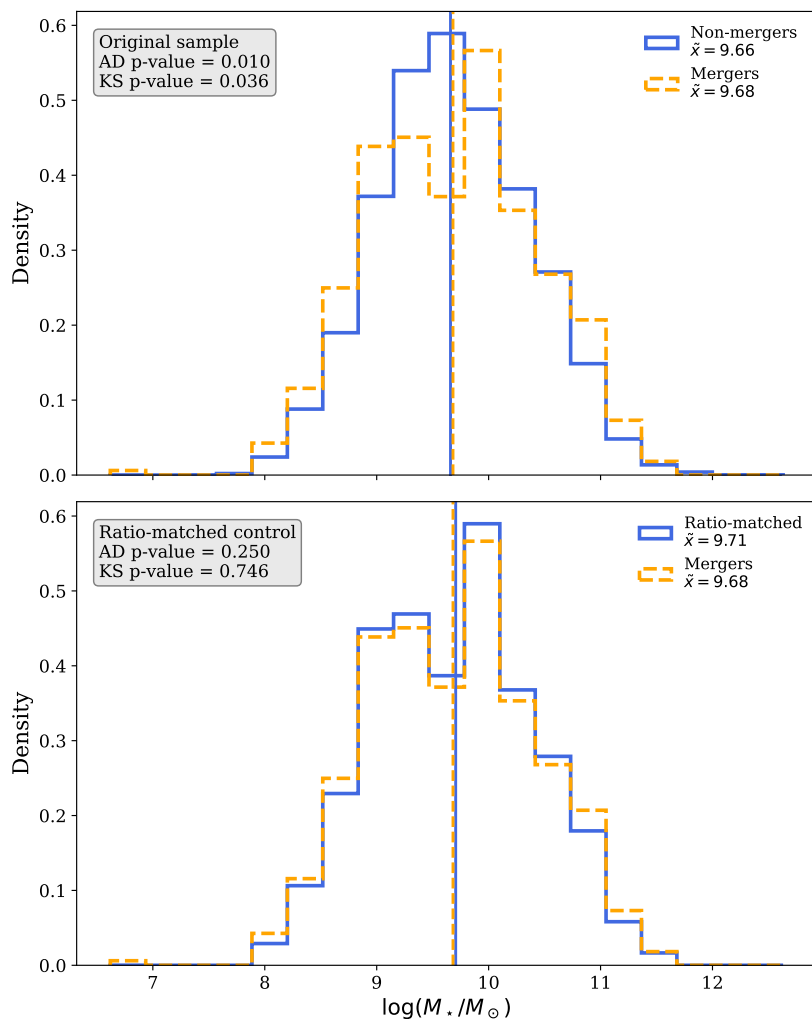


Fig. C.1. Stellar mass distributions of merging and non-merging galaxies. The top panel shows the original samples, which are similar in shape but statistically different (AD and KS tests). The bottom panel shows a ratio-matched control sample, where non-mergers are randomly down-sampled in stellar-mass bins to reproduce the merger mass distribution without enforcing equal sample sizes. The result corresponds to one realization from 1000 Monte Carlo resamplings. Controlling for stellar mass does not change the conclusions.

Appendix D: Alignment of mergers with filaments in the entire cluster sample

Figures D.1 and D.2 present the clusters used in our analysis, ordered by increasing p -value. The first figure shows the spatial distribution of merger candidates along the filaments. The second figure displays the corresponding distributions of distances to the filament for each cluster.

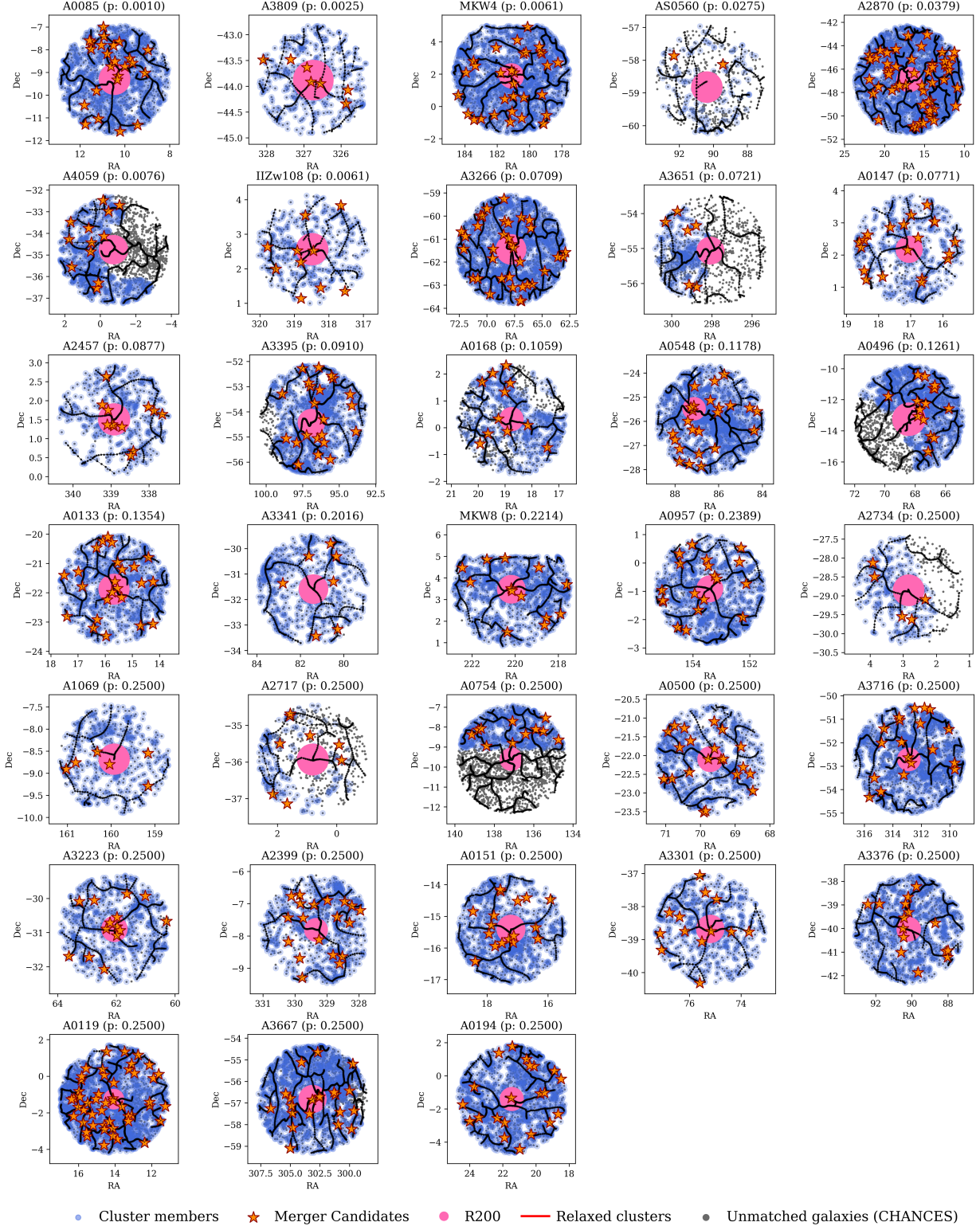


Fig. D.1. Distribution of galaxy-galaxy mergers (orange stars) across the 33 clusters in our sample. Black lines represent filaments, the pink circle denotes the virial radius (R_{200}), and blue points correspond to the general cluster galaxy population. For visualization purposes, grey points represent all unmatched cluster members from the CHANCES catalogue, which were not included in the statistical analysis.

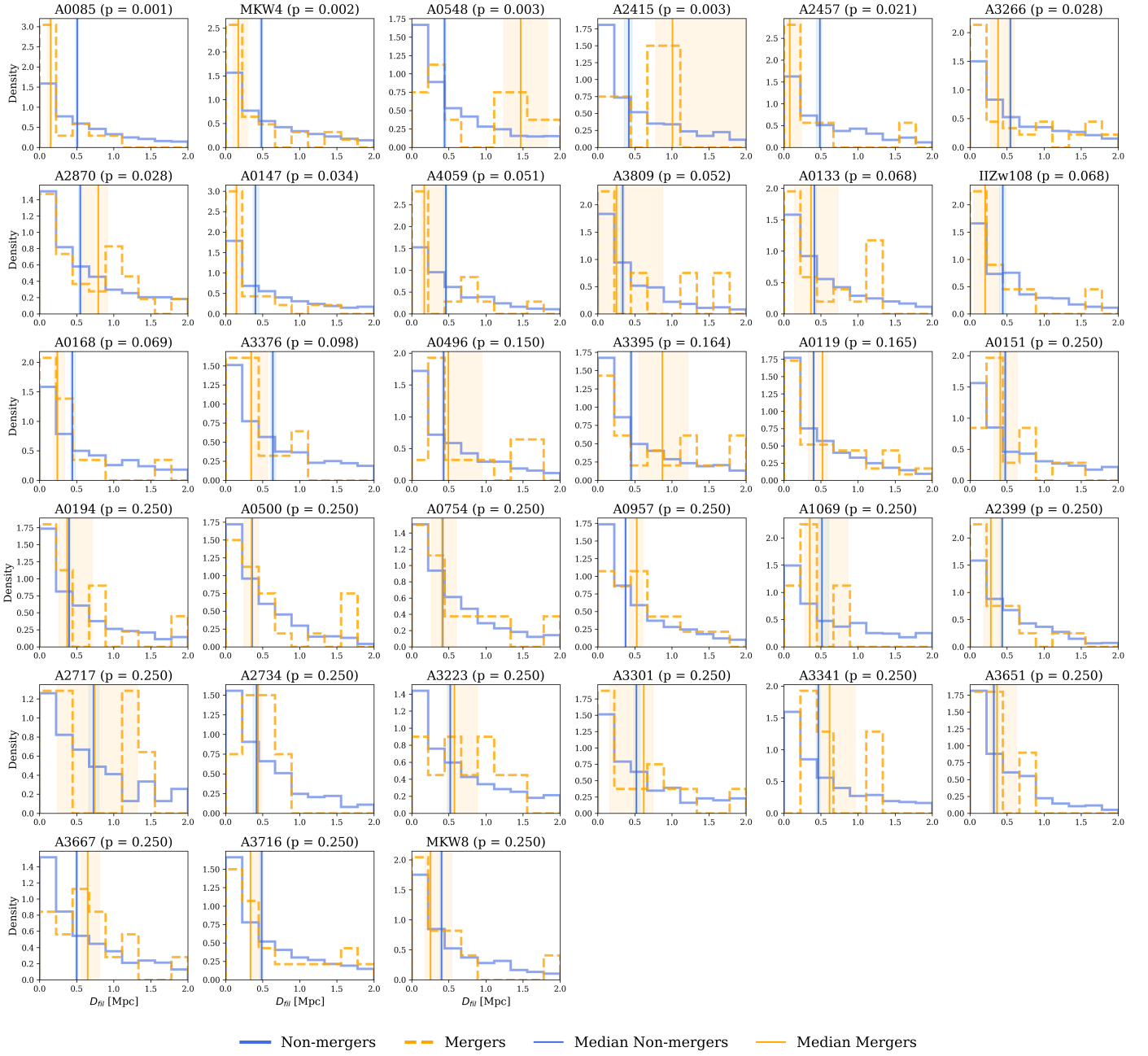


Fig. D.2. Normalized distribution of the nearest distances to filaments for galaxy mergers located outside $1 \times R_{200}$ in the 33 galaxy clusters (orange dashed line), compared to the non-merging cluster galaxy population outside $1 \times R_{200}$ of each respective cluster (blue dotted line). Error bars correspond to Poisson uncertainties in each bin, while vertical lines mark the median of each distribution. Shaded regions indicate the 68% bootstrap confidence intervals (percentiles 16–84) around the median. Clusters are ordered from lowest to highest p-value, where a lower p-value indicates stronger evidence of a difference between the distributions. Distances to filaments are truncated at 2 Mpc to emphasize the vicinity where most merger candidates are found, although the full distributions extend up to ~ 4 Mpc.